

Zero-bias spin separation

Sergey D. Ganichev¹, Vasily V. Bel'kov^{1,2}, Sergey A. Tarasenko², Sergey
N. Danilov¹, Stephan Giglberger¹, Christoph Hoffmann¹, Eougenious L. Ivchenko²,
Dieter Weiss¹, Werner Wegscheider¹, Christian Gerl¹, Dieter Schuh¹,
Joachim Stahl¹, Joan De Boeck³, Gustaaf Borghs³, & Wilhelm Prettl¹

¹*Fakultät Physik, University of Regensburg, 93040, Regensburg, Germany*

²*A.F. Ioffe Physico-Technical Institute,*

Russian Academy of Sciences, 194021 St. Petersburg, Russia and

³*IMEC, Kapeldreef 75, B-3001 Leuven, Belgium*

(Dated: August 27, 2018)

PACS numbers: 73.21.Fg, 72.25.Fe, 78.67.De, 73.63.Hs

Spin-orbit coupling provides a versatile tool to generate and to manipulate the spin degree of freedom in low-dimensional semiconductor structures. The spin Hall effect, where an electrical current drives a transverse spin current and causes a nonequilibrium spin accumulation observed near the sample boundary^{1,2}, the spin-galvanic effect, where a nonequilibrium spin polarization drives an electric current³, or the reverse process, in which an electrical current generates a nonequilibrium spin polarization^{4,5,6}, are all consequences of spin-orbit coupling. In order to observe a spin Hall effect a bias driven current is an essential prerequisite. The spin separation is caused via spin-orbit coupling either by Mott scattering (extrinsic spin Hall effect) or by spin splitting of the band structure (intrinsic spin Hall effect). Here we provide evidence for an elementary effect causing spin separation which is fundamentally different from that of the spin Hall effect. In contrast to the spin Hall effect it does not require an electric current to flow: It is spin separation achieved by spin-dependent scattering of electrons in media with suitable symmetry. We show that by free carrier (Drude) absorption of terahertz radiation spin separation is achieved in a wide range of temperatures from liquid helium up to room temperature. Moreover the experimental results give evidence that simple electron gas heating by any means is already sufficient to yield spin separation due to spin-dependent energy relaxation processes of nonequilibrium carriers.

Scattering of electrons involves a transition from a state with wavevector \mathbf{k} to a state with wavevector \mathbf{k}' which is usually considered to be spin-independent. However, in gyrotropic media, e.g. GaAs quantum wells or heterojunctions, spin-orbit interaction adds an asymmetric spin-dependent term to the scattering probability⁷. The asymmetric spin-dependent

scattering matrix element is linear in wavevector⁸ \mathbf{k} and the Pauli spin matrices $\boldsymbol{\sigma}$. Microscopically this term is caused by structural inversion asymmetry (SIA) and/or bulk inversion asymmetry (BIA). While the asymmetry of electron scattering can cause spin currents to flow, it does not modify the energy spectrum.

A process actuating spin separation is illustrated in Fig. 1 (a) and involves Drude absorption of radiation. Drude absorption is caused by indirect intraband optical transitions and includes a momentum transfer from phonons or impurities to electrons to satisfy momentum conservation. Figure 1 (a) sketches the process of Drude absorption via virtual states for a spin-up subband ($s = +1/2$, left panel) and a spin-down subband ($s = -1/2$, right panel) of a quantum well containing a two-dimensional electron gas.

Vertical arrows indicate optical transitions from the initial state with electron wavevector $k_x = 0$ while the horizontal arrows describe an elastic scattering event to a final state with either positive or negative electron wavevector k'_x . While, for simplicity of illustration, we have only shown transitions starting from $k_x = 0$, the arguments given here are valid for arbitrary k_x . Due to the spin dependence of scattering, transitions to positive and negative k'_x -states occur with different probabilities. This is indicated by horizontal arrows of different thicknesses. Since the asymmetric part of electron scattering is proportional to components of the vector product $[\boldsymbol{\sigma} \times \mathbf{k}']$ higher and lower probabilities for scattering to positive or negative k'_x get inverted for a spin-down subband compared to that of a spin-up subband⁹. Similarly, also relaxation of excited carriers is asymmetric as is sketched in Fig. 1 (b). Since this mechanism causes only a polarization independent background signal in the experiments discussed below, the discussion will first be focused on the mechanism displayed in Fig. 1 (a).

The asymmetry causes an imbalance in the distribution of photoexcited carriers in the spin subbands ($s = \pm 1/2$) between positive and negative k'_x states, which in turn yields

electron flows $\mathbf{i}_{\pm 1/2}$ within each spin subband¹⁰. However, the charge currents, $\mathbf{j}_+ = e\mathbf{i}_{1/2}$ and $\mathbf{j}_- = e\mathbf{i}_{-1/2}$, where e is the electron charge, have opposite directions because $\mathbf{i}_{+1/2} = -\mathbf{i}_{-1/2}$ and therefore cancel each other. Nevertheless, a spin current $\mathbf{J}_{\text{spin}} = \frac{1}{2}(\mathbf{i}_{+1/2} - \mathbf{i}_{-1/2})$ is generated since electrons with spin-up and spin-down move in opposite directions. This leads to a spatial spin separation and spin accumulation at the edges of the sample.

By application of a magnetic field which polarizes spins, the spin current gets detected as charge current. This is analogous to spin-dependent scattering in transport experiments: Mott scattering of unpolarized electrons causes the extrinsic spin Hall effect, whereas in a spin polarized electron gas a charge current, the anomalous Hall effect, can be observed. In a spin polarized system, the two fluxes $\mathbf{i}_{\pm 1/2}$, which are proportional to the spin-up and spin-down free carrier densities, $n_{\pm 1/2}$, cease compensating each other and yield a net electric current¹¹

$$\mathbf{j} = e(\mathbf{i}_{+1/2} + \mathbf{i}_{-1/2}) = 4eS\mathbf{J}_{\text{spin}} , \quad (1)$$

where $S = \frac{1}{2}(n_{+1/2} - n_{-1/2})/(n_{+1/2} + n_{-1/2})$ is the average spin. An external magnetic field \mathbf{B} results in different populations of the two spin subbands due to the Zeeman effect. In equilibrium the average spin is given by

$$\mathbf{S} = -\frac{g\mu_B\mathbf{B}}{4\bar{\varepsilon}} . \quad (2)$$

Here g is the electron effective g -factor, μ_B the Bohr magneton, $\bar{\varepsilon}$ the characteristic electron energy being equal to the Fermi energy ε_F , or to the thermal energy k_BT , for a degenerated and a non-degenerated two-dimensional electron gas, respectively.

In order to demonstrate the existence of the spin current due to asymmetric scattering described above we carry out the following experiment: Drude absorption is achieved using linearly polarized terahertz radiation directed along the growth direction of a (001)-oriented

heterostructures. The equilibrium spin polarization is obtained by an in-plane magnetic field \mathbf{B} , which shifts the two parabolas of Fig. 1 (a) vertically by $\pm g\mu_B B/2$. The photocurrent is measured both in the directions perpendicular and parallel to the magnetic field. The chosen experimental conditions exclude other effects known to cause photocurrents: Since linearly polarized radiation is used, all helicity dependent spin photocurrents, such as the spin-galvanic effect⁴ and the circular photogalvanic effect¹³, are absent. In addition, a possible photon drag effect and the linear photogalvanic effect are forbidden by symmetry for normal incidence on (001)-grown heterostructures¹⁴.

The experiments are carried out on both, MBE-grown (001)-oriented *n*-type GaAs/AlGaAs and InAs/AlGaSb two-dimensional structures. The parameters of the investigated samples are given in Table I. Two pairs of ohmic contacts at the center of the sample edges and lying along the $x \parallel [1\bar{1}0]$ and $y \parallel [110]$ directions have been prepared to measure the photocurrent (see inset in Fig. 2). A high power pulsed molecular terahertz laser has been used as radiation source delivering 100 ns pulses with radiation power P up to 1 kW. Several wavelengths between 77 and 496 μm have been selected using NH_3 , D_2O and CH_3F as active media¹⁴. The samples are irradiated under normal incidence, along the growth direction. The terahertz radiation causes indirect optical transitions within the lowest size-quantized subband. Since the energy $\hbar\omega$ of a terahertz photon is much smaller than the GaAs and InAs band gap as well as the energy separation between the lowest lying filled subband and the first excited subband, direct optical transitions are absent. In experiments the angle between the polarization plane of the linearly polarized light and the magnetic field is varied. This is achieved by placing a metal grid polarizer in a circularly polarized beam obtained by a crystalline quartz $\lambda/4$ -plate. Rotation of the metal grid enables us to vary, at constant intensity, the angle $\alpha = 0^\circ \div 180^\circ$ between the x axis and the plane of

linear polarization of the light incident upon the sample (see inset in the upper panel of Fig. 3). The external magnetic field with a maximum field strength of $B = 0.6$ T is applied parallel to the heterostructure interface along $[110]$ crystallographic direction. The electric current generated by the light in unbiased devices is measured via the voltage drop across a $50\ \Omega$ load resistor in a closed circuit configuration. The voltage is recorded with a storage oscilloscope.

Irradiation of the samples at zero magnetic field does not lead – as expected – to any current. A photocurrent response is obtained only when the magnetic field is applied. The measured current pulses of 100 ns duration reflect the corresponding laser pulses. As described by Eqs. (1) and (2) the current increases linearly with B_y due to the increasing spin polarization (see upper panel of Fig. 4) and changes sign upon reversal of \mathbf{B} . Corresponding data will be discussed below for the different samples. The temperature and polarization dependences of the current were measured in all samples for two directions: along and perpendicular to the in-plane magnetic field. Figure 2 shows the typical temperature dependence of the photocurrent measured in the direction perpendicular to the magnetic field and, as shown in the inset, with the radiation also polarized perpendicularly to the magnetic field. While the photocurrent is constant at low temperatures it decreases as $1/T$ at temperatures above 100 K. As we show below the peculiar temperature dependence is direct evidence that the current is driven by the spin polarization given by Eq. (2).

Before we discuss the corresponding microscopic origin in more detail we present measurements of polarization dependences of the current components perpendicular (Fig. 3, upper panel) and parallel (Fig. 3, lower panel) to the applied magnetic field, B_y . The polarization dependence of the current j in transverse geometry can be fitted by $j_x = j_1 \cos 2\alpha + j_2$, and by $j_y = j_3 \sin 2\alpha$ for the longitudinal geometry. The overall polarization dependences of the

photocurrent remain the same independently of temperature and wavelength. The increase of the radiation wavelength at constant intensity results in an increased signal strength. The wavelength dependence for both transverse and longitudinal configurations is described by $j \propto \lambda^2$ in the whole range of wavelengths used (see inset in Fig. 3, lower panel) which corresponds to the spectral behaviour of Drude absorption, $\eta(\omega) \propto 1/\omega^2$ at $\omega\tau_p \gg 1$ (see¹⁵). Here $\eta(\omega)$ is the absorbance of heterostructure at the radiation frequency ω .

The fact that an offset j_2 is observed for the transverse geometry only is in accordance with the phenomenological theory of magnetic field induced photocurrents¹⁶. Under normal incidence of linearly polarized radiation and in the presence of an in-plane magnetic field, B_y , the current components are described by

$$j_x = C_1 B_y (e_x^2 - e_y^2) I + C_2 B_y I, \quad (3)$$

$$j_y = C_3 B_y e_x e_y I, \quad (4)$$

where I and \mathbf{e} are the light intensity and polarization vector, respectively. The parameters C_1 to C_3 are coefficients determined by the C_{2v} symmetry relevant for (001)-oriented structures. The polarization independent offset is described by the second term in the right hand side of Eq. (3) and is present for the transverse geometry only. The only visible consequence of this contribution is the offset in the upper panel of Fig. 3. The other terms in the right hand sides of Eqs. (3) and (4) yield polarization dependences in full agreement with experiments.

All experimental features, i.e., the temperature and polarization dependences, are driven by the spin degree of freedom: For fixed polarization for both excitation (Fig. 1 (a)) and relaxation (Fig. 1 (b)) mechanisms the current is proportional to the frequency dependent absorbance $\eta(\omega)$, momentum relaxation time τ_p , light intensity I and average spin S : $j \propto \eta(\omega)I\tau_p S$. Such type of expression, which determines the temperature dependence, is valid

for fixed scattering mechanism, e.g. phonon or impurity scattering. To corroborate this claim and obtain the polarization dependence microscopically we present the results of the corresponding theory for impurity scattering.

A consistent description of magneto-induced photocurrent can be developed within the framework of the spin-density matrix. The scattering asymmetry induced contribution to the magneto-induced photocurrents is given by

$$\mathbf{j} = \sum_{s\mathbf{k}} e \mathbf{v}_{\mathbf{k}} \delta f_{s\mathbf{k}} = e \frac{2\pi}{\hbar} \sum_{s\mathbf{k}\mathbf{k}'} \tau_p (\mathbf{v}_{\mathbf{k}} - \mathbf{v}_{\mathbf{k}'}) |M_{s\mathbf{k},s\mathbf{k}'}|^2 (f_{s\mathbf{k}'} - f_{s\mathbf{k}}) \delta(\varepsilon_{\mathbf{k}} - \varepsilon_{\mathbf{k}'} - \hbar\omega). \quad (5)$$

Here $\mathbf{v}_{\mathbf{k}} = \hbar\mathbf{k}/m^*$ is the electron velocity, m^* the effective electron mass, $\delta f_{s\mathbf{k}}$ the fraction of the carrier distribution function stemming from optical transitions in the spin subband s , $M_{s\mathbf{k},s\mathbf{k}'}$ the matrix element of the indirect optical transition, $f_{s\mathbf{k}}$ the equilibrium distribution function, $\varepsilon_{\mathbf{k}} = \hbar^2 k^2/2m^*$ the electron kinetic energy for in-plane motion, and s an index enumerating subbands with spin states $\pm 1/2$ along the direction of the external magnetic field.

To first order in spin-orbit interaction the compound matrix element for the indirect optical transitions via impurity scattering has the form¹⁷

$$M_{\mathbf{k},\mathbf{k}'} = \frac{eA}{c\omega m^*} \mathbf{e} \cdot (\mathbf{k} - \mathbf{k}') V_{\mathbf{k}\mathbf{k}'} - 2 \frac{eA}{c\hbar} \sum_{\alpha\beta} V_{\alpha\beta} \sigma_{\alpha} e_{\beta}. \quad (6)$$

Here $\mathbf{A} = A\mathbf{e}$ is the vector potential of the electromagnetic wave, c the light velocity and $V_{\mathbf{k}\mathbf{k}'}$ the scattering matrix element given by¹⁸

$$V_{\mathbf{k}\mathbf{k}'} = V_0 + \sum_{\alpha\beta} V_{\alpha\beta} \sigma_{\alpha} (k_{\beta} + k'_{\beta}), \quad (7)$$

where the term V_0 describes the conventional spin independent scattering and the term proportional to the second rank pseudo-tensor $V_{\alpha\beta}$ yields the asymmetric spin-dependent contribution linear in \mathbf{k} and responsible for the effects described here. The first term on

the right side of Eq. (6) describes transitions involving virtual intermediate states in the conduction band while the second term corresponds to transitions via virtual intermediate states in the valence band.

For C_{2v} point-group symmetry there are only two non-zero components of the tensor $V_{\alpha\beta}$: V_{xy} and V_{yx} . By using Eqs. (5) to (7) an expression for the electric current \mathbf{j} can be derived. We consider the free-carrier absorption to be accompanied by electron scattering from short-range static defects and assume therefore that the matrix element V_0 and the coefficients $V_{\alpha\beta}$ are wavevector independent. As well as in experiment we consider linearly polarized light at normal incidence and an in-plane magnetic field B_y resulting in an average spin S_y . Then currents parallel and perpendicular to the magnetic field can be written as

$$j_x = -2(e_x^2 - e_y^2) V_{yx} S_y \frac{e\tau_p}{\hbar V_0} I\eta(\omega) , \quad (8)$$

$$j_y = -4e_x e_y V_{xy} S_y \frac{e\tau_p}{\hbar V_0} I\eta(\omega) , \quad (9)$$

where the photon energy $\hbar\omega$ is assumed to be smaller than the characteristic energy $\bar{\epsilon}$. Note, that the polarization independent part of Eq. (3) is missing here as the above theory does not contain the relaxation process, sketched in Fig. 1 (b), which is responsible for the background signal of Fig. 3 (a).

Equations (8) and (9) contain the polarization dependence for transverse and longitudinal orientation, respectively, given by

$$e_x^2 - e_y^2 = \cos 2\alpha , \quad 2e_x e_y = \sin 2\alpha . \quad (10)$$

The observed polarization dependences are in a full agreement with Eqs. (8), (9) and (10) (see fits in Fig. 3). It should be noted that the polarization behaviour of j_x and j_y depends neither on temperature nor on wavelength. It is solely described by Eqs. (3) and (4) and does not depend on specific scattering mechanism of Drude absorption.

However, the different scattering mechanisms involved in Drude absorption are reflected in the temperature dependence of the photocurrent displayed in Fig. 2. While impurity scattering prevails at low temperatures, phonon scattering takes over for $T > 100$ K and is then the dominant scattering mechanism¹⁹. For temperatures up to about 25 K the photocurrent is constant though both, mobility and carrier density change significantly. Since, Drude absorption, $\eta(\omega) \propto n_s/\tau_p$ at $\omega\tau_p \gg 1$ (see¹⁵) and at low temperatures $S \propto 1/\varepsilon_F \propto 1/n_s$ (see Eq. (2)), the current $j/I \propto \tau_p \eta(\omega) S$ is constant and independent of τ_p and n_s . In additional experiments we changed the carrier density at 4.2 K by visible and near infrared light. For the sample 1, e.g., the carrier density (mobility) increases from $1.3 \cdot 10^{11} \text{ cm}^{-2}$ ($1.7 \cdot 10^6 \text{ cm}^2/\text{Vs}$) to $3.0 \cdot 10^{11} \text{ cm}^{-2}$ ($4.1 \cdot 10^6 \text{ cm}^2/\text{Vs}$) after illumination at low T . Though both n_s and τ_p increase by a factor of 2, the photocurrent remains unchanged, thus confirming the above arguments. In contrast, for $T > 100$ K the carrier density n_s is roughly constant (saturation region) but S is now $\propto 1/k_B T$, see Eq. (2). Hence, the current j is proportional to n_s/T and becomes temperature dependent in accordance with our experimental observation. Fits to the data in the low- T and high- T regimes are shown as solid lines in Fig. 2. In the intermediate range of temperatures between 25 K and 100 K, where a rising current is observed, such simple analysis fails. In this range the scattering mechanism, responsible for the spin currents, changes from impurity dominating to phonon dominating. This transition region is not yet theoretically treated and out of scope of the present letter.

The experiments, carried out on different samples, are summarized in Fig. 4. Using the arrangement of upper panel in Fig. 3 for two fixed polarization directions, $\alpha = 0^\circ$ and $\alpha = 90^\circ$, we obtain a linear increase of the corresponding photocurrent, shown in the upper panel of Fig. 4. By adding and subtracting the currents of both orientations the coefficients

j_1 (polarization dependent amplitude) and j_2 (polarization independent background) can be extracted. Corresponding results of j_1 (lower left panel) and j_2 (lower right panel) for four different samples are shown. Due to the larger g -factor of sample 4 (InAs QW), causing larger average spin S , the currents are largest for this sample. The other three samples are GaAs based heterostructures which differ in structural inversion asymmetry. Sample 1 is a heterojunction (see Table I) which, due to triangular confinement potential, is expected to have the strongest SIA contribution. Samples 2 and 3 are quantum wells of the same width asymmetrically and symmetrically modulation doped, with larger and smaller strength of SIA, respectively. The fact that with decreasing strength of the SIA coupling coefficient (from sample 1 to 3) the currents become smaller is in excellent agreement with our picture of asymmetric scattering driven currents. The coupling strength constant controls the current via $V_{\alpha\beta}$ in Eqs. (8), (9) and equivalent expressions for other scattering mechanisms: The larger the coupling strength the larger is the effect of asymmetric scattering.

Finally we would like to address the role of spin-dependent relaxation, sketched in Fig. 1 (b). The absorption of radiation leads to an electron gas heating. Due to the spin-dependent asymmetry of scattering energy relaxation rates for positive and negative k_x within each spin subband are nonequal as indicated by bent arrows of different thicknesses. Thus, spin flows $i'_{\pm 1/2}$ are generated in both spin subbands. Like for Drude excitation spin separation takes place and applying a magnetic field results in a net electric current. As indicated in Fig. 1 (a) and Fig. 1 (b) excitation and relaxation induced currents flow in opposite directions. Experimentally this is observed for all samples: j_1 and j_2 for each sample have consistently opposite signs. As mentioned before j_1 stands for polarization dependent part of the photocurrent due to excitation, while j_2 is polarization independent and due to relaxation.

Summarizing, we emphasize that all central experimental features of the terahertz photocurrent, namely, magnetic field, temperature, mobility, and concentration dependences provide evidence that the observed effect is solely determined by the spin degree of freedom. Furthermore our observations suggest that heating of the electron gas by any means (microwaves, voltage etc.) is sufficient to generate spin currents. Our results demonstrate that spin-dependent scattering provides a new tool for spin manipulation.

Acknowledgements

We would like to thank Imke Gronwald for preparation of the samples. This work was supported by the DFG via Project GA-501/5, Research Unit FOR370 and Collaborative Research Center SFB689, the RFBR and programs of the RAS. S.G. thanks the HBS and S.A.T. the Foundation “Dynasty” - ICFPM and the President Grant for young scientists for support.

-
- ¹ Kato Y., Myers R.C., Gossard A.C. & Awschalom D., Observation of the spin Hall effect in semiconductors, *Science* **306**, 1910 (2004).
 - ² Wunderlich J., Kaestner B., Sinova J. & Jungwirth T., Experimental observation of the spin-hall effect in a two-dimensional spin-orbit coupled semiconductor system, *Phys. Rev. Lett.* **94**, 047204 (2005).
 - ³ Ganichev S.D. *et al.*, Spin-galvanic effect, *Nature (London)* **417**, 153 (2002).
 - ⁴ Ganichev S.D. *et al.*, Can current orient spins?, cond-mat/0403641 (2004), and Ganichev S.D. *et al.*, Electric current induced spin orientation in quantum well structures, *J. Magn. & Magn. Materials* **300**, 127 (2006).

- ⁵ Silov A.Yu. *et al.*, Current-induced spin polarization at a single heterojunction, *Appl. Phys. Lett.* **85**, 5929 (2004).
- ⁶ Kato Y., Myers R.C., Gossard A.C. & Awschalom D., Current-induced spin polarization in strained semiconductors, *Phys. Rev. Lett.* **93**, 176601 (2004).
- ⁷ Spin-dependent scattering processes responsible for the zero-bias spin separation and for the extrinsic spin Hall effect, in spite of the vocabulary similarity, are principally different. While odd in \mathbf{k} scattering, does not require directed electron motion and needs sufficiently low symmetry of material, skew scattering driving extrinsic spin Hall effect is due to average carrier velocity and can be present even in highly symmetric materials.
- ⁸ In fact all terms odd in \mathbf{k} , including \mathbf{k} -cubic terms, may also contribute to spin dependent asymmetric scattering. In the present paper we limit our consideration to the lowest order term which is linear in \mathbf{k} .
- ⁹ Note that we assumed $k_x = 0$, and structural inversion asymmetry only.
- ¹⁰ Tarasenko S.A. & Ivchenko E.L., Pure spin photocurrents in low-dimensional structures, *Pis'ma Zh. Eksp. Teor. Fiz.* **81**, 292 (2005) [*JETP Lett.* **81**, 231 (2005)].
- ¹¹ Here we neglect effects of electron-electron interaction on a spin transport recently addressed in ¹².
- ¹² Weber C.P. *et al.*, Observation of spin Coulomb drag in a two-dimensional electron gas, *Nature* **437**, 1330 (2005).
- ¹³ Ganichev S.D. *et al.*, Conversion of spin into directed electric current in quantum wells, *Phys. Rev. Lett.* **86**, 4358 (2001).
- ¹⁴ Ganichev S.D. & Prettl W., *Intense Terahertz Excitation of Semiconductors*, Oxford University Press, Oxford (2006).

- ¹⁵ Seeger K., *Semiconductor Physics*, Springer, Wien (1997).
- ¹⁶ Bel'kov V.V. *et al.*, Magneto-gyrotropic photogalvanic effects in semiconductor quantum wells, *J. Phys.: Condens. Matter* **17**, 3405 (2005).
- ¹⁷ Tarasenko S.A., Spin orientation of a two-dimensional electron gas by a high-frequency electric field, *Phys. Rev. B* **73**, 115317 (2006).
- ¹⁸ Ivchenko E.L. & Pikus G.E., Optical orientation of free carriers spins and photogalvanic effects in gyrotropic crystals, *Izv. Akad. Nauk SSSR (ser. fiz.)* **47**, 2369 (1983) [*Bull. Acad. Sci. USSR, Phys. Ser.*, **47**, 81 (1983)].
- ¹⁹ Kelly M.J., *Low-Dimensional Semiconductors*, Clarendon Press, Oxford (1995).

TABLE I: Parameters of investigated samples. Mobility and electron sheet density data are obtained at 4.2 K in the dark.

sample	material	QW width	spacer 1	spacer 2	mobility	density
		\AA	\AA	\AA	cm^2/Vs	cm^{-2}
#1	GaAs/AlGaAs	∞	500		$1.7 \cdot 10^6$	$1.3 \cdot 10^{11}$
#2	GaAs/AlGaAs	300	700		$3.6 \cdot 10^6$	$1.3 \cdot 10^{11}$
#3	GaAs/AlGaAs	300	700	1000	$3.4 \cdot 10^6$	$1.8 \cdot 10^{11}$
#4	InAs/AlGaSb	150			$2.0 \cdot 10^4$	$1.3 \cdot 10^{12}$

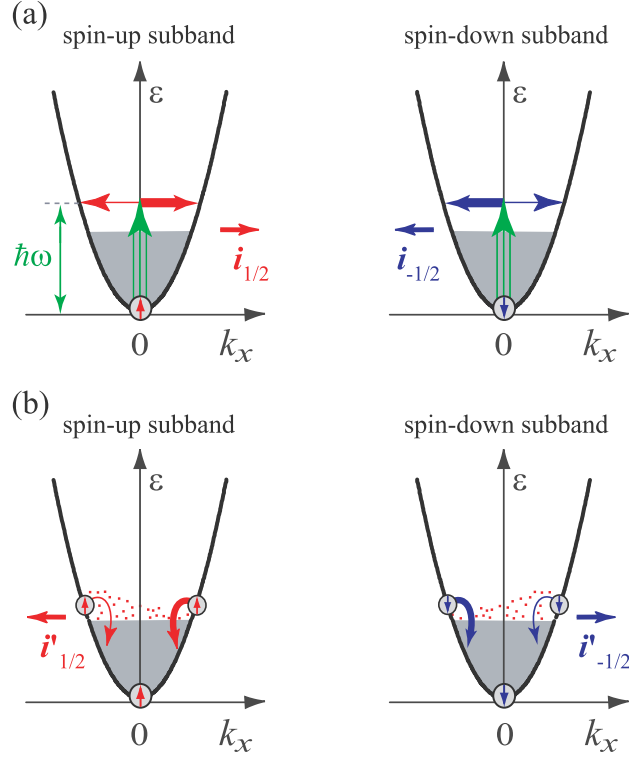


FIG. 1: Microscopic origin of the zero-bias spin separation due to linear in \mathbf{k} and the Pauli spin matrices $\boldsymbol{\sigma}$ terms in electron scattering, see Eq. (7). (a) caused by excitation asymmetry and (b) due to spin-dependent energy relaxation. It is assumed that scattering for spin-up subband has larger probability for positive k_x than that for negative k_x and vice versa for spin-down subband.

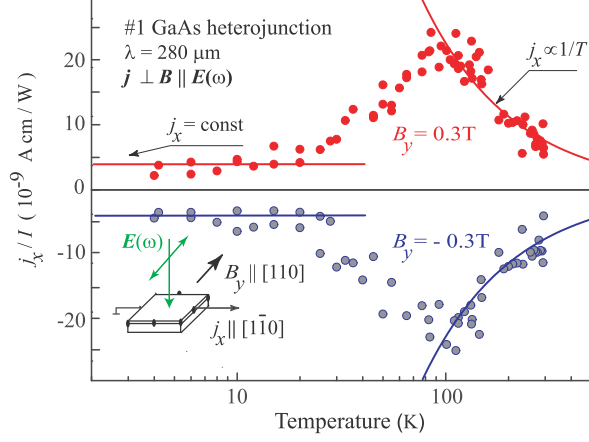


FIG. 2: Photocurrent j_x in a (001)-grown GaAs/AlGaAs heterojunction as a function of sample temperature for two opposite polarities of the magnetic field. The photocurrent $\mathbf{j} \perp \mathbf{B} \parallel y$ is excited by normally incident linearly polarized radiation of $\lambda = 280 \mu\text{m}$. Full lines are fits to $j_x = \pm \text{const}$ at low T and $j_x \propto \pm 1/T$ at high T . The inset shows the geometry of the experiment.

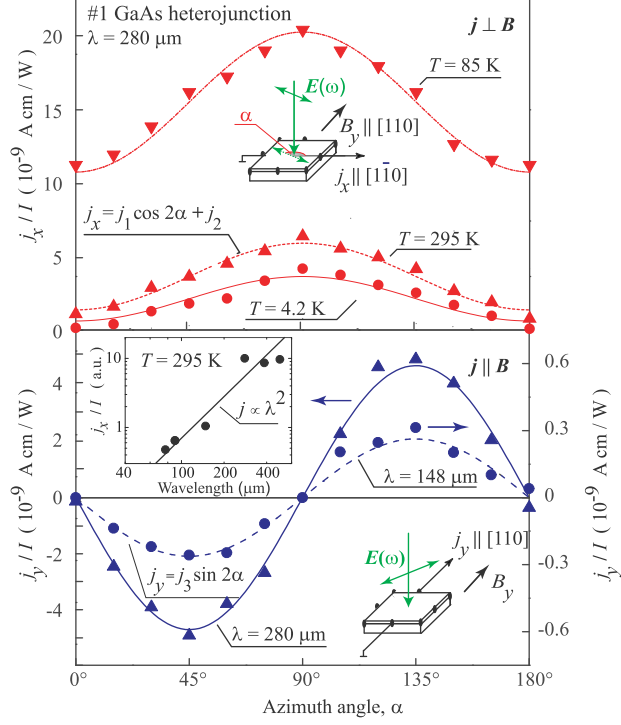


FIG. 3: Photocurrents in a (001)-grown GaAs/AlGaAs heterojunction as a function of the azimuth angle α . Data are obtained for normal incidence of linearly polarized radiation measured for $B = 0.3$ T. Upper panel: photocurrent $\mathbf{j} \perp \mathbf{B} \parallel y$ at $\lambda = 280 \mu\text{m}$ and various temperatures. Lines are fitted according to $j_x = j_1 \cos 2\alpha + j_2$, see Eqs. (3), (8) and (10). Lower panel: photocurrent $\mathbf{j} \parallel \mathbf{B} \parallel y$ measured at room temperature for two wavelengths $\lambda = 148$ and $280 \mu\text{m}$. Lines are fitted according to $j_y = j_3 \sin 2\alpha$, see Eqs. (9) and (10). Insets show the experimental geometries. An additional inset in lower panel demonstrates the wavelength dependence of the signal for the transverse geometry. The full line shows $j_x \propto \lambda^2$.

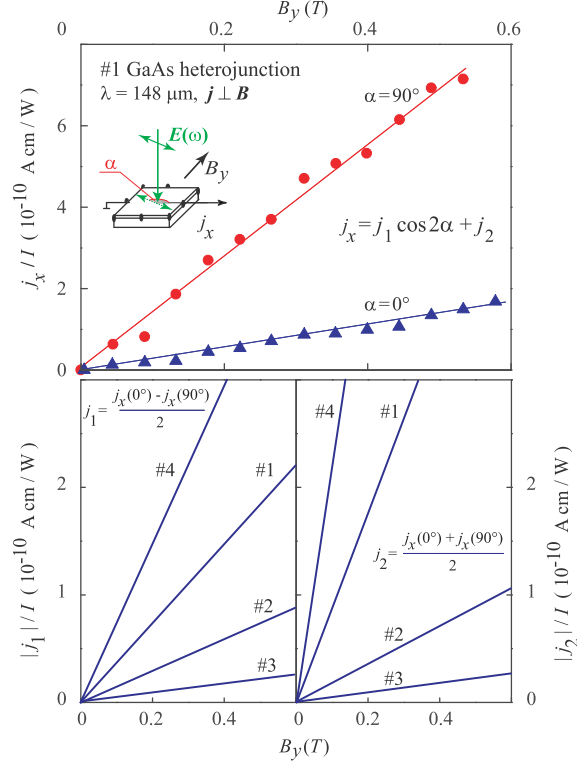


FIG. 4: Magnetic field dependence of the transversal photocurrent. Upper panel: $j_x(B)$ measured in sample 1 at room temperature for two polarization states. Lower panels: $j_1(B)$ (left panel) and $j_2(B)$ (right panel) obtained by adding and subtracting the currents corresponding to excitations of both polarizations for various samples.